GeoGravGOCE

Geoid and Gravity Field Modelling by GOCE Satellite Gradients and Terrestrial Data

WP 1: Project management
TSK1200: Reporting and action list update

DELIVERABLE
DL1210.1: 1st Semi-annual progress report

Distribution List			
HFRI		**AUTH Research Committee**	
HFRI DL Office	1	RC AUTH DL Office	1

Table of Contents

Abstract

This report refers to management activities of the GeoGravGOCE project and more precisely to the first (July 2020) semi-annual progress report by the project team to the HFRI DL office. All activities, which were carried out up to the reporting period, are outlined and details on the actions to be taken within the next 6 months reporting period are given.

H.F.R.I.
Hellenic Foundation for
Research & Innovation

GeoGravGOCE

Ref: Con. Nr. 3488
Version: 1.0
Date: 1.21.2020
Page: 8/37

List of Figures

List of Tables

Acronyms

DL	Deliverable
EFRF	Earth Fixed Reference Frame
ES	Earth Surface
ESA	European Space Agency
FIR	Finite Impulse Response
GGMs	Global Geopotential Models
GRF	Gradiometer Reference Frame
GSRT	General Secretariat for Research and Technology
GUI	Graphical User Interface
HFRI	Hellenic Foundation for Research and Innovation
ICGEM	International Center for Global Earth Models
IIR	Infinite Impulse Response
IRF	Inertial Reference Frame
LNOF	Local North Oriented Frame
MO	Mean Orbit
MRA	Multi-Resolution Approximation
PSD	Power Spectral Density
SGG	Satellite Gravity Gradiometry
TSK	Task
WL	Wavelet
WP	Work Package
WPS	Work Package Structure
w.r.t.	with respect to

1.

GeoGravGOCE project kick-off meeting

1.1 Outline of the deliverable

This report refers to management activities of the GeoGravGOCE project and more precisely to the first (July 2020) semi-annual progress report by the project team to the HFRI DL office. All activities, which were carried out up to the reporting period, are outlined and details on the actions to be taken within the next 6 months reporting period are given.

1.2 Activities and progress during the first six months of the project

During the first six months of the GeoGravGOCE project, the main managerial and research activities needed have been carried out. These refer to the preparation of the semi-annual report and the reports on the methodologies for: a) the pre-processing of the data, b) the transformation of the original SGGs from GRF to LNOF, c) the various options of filtering, d) the estimation of gravity gradients from GGMs e) the data reduction and selective filtering methods and f) the development of the software GUI platform.

1.3 Pre-Processing

The GeoGravGOCE project analyses the GOCE Level 2 products, accessed from the GOCE Virtual on-line Archive (http://eo-virtual-archive1.esa.int/GOCEL2.html). In the pre-processing, all the available data, EGG_NOM_2 and SST_PSO_2, were parsed using the GOCEPARSER program (Arsov 2012) in order to extract the Level 2 data from the XML structure into a conventional text file in columnar format, easily readable from the Matlab. The GOCEPARSER's output format are *.sgg files for the NOM data, which contain the gravity gradients and *.kin and *.qat for the PSO data, which include the satellite's kinematic orbit information as well as the quaternions needed for the transformation from the EFRF reference system to IRF.

All mention formed outputs were further processed in Matlab. A significant issue was the dimensions of the data, which were not equal. Therefore, the length of the NOM data was compared and reduced based on the PSO data. After this pre-processing, all the Level 2 GOCE data were ready for further processing according to the project's requirements.

1.4 Transformation of the original SGGs from GRF to LNOF

After the pre-processing of the initial data, a transformation of the original SGGs from the Gradiometer Reference Frame (GRF) to the Local North Oriented Frame (LNOF) was applied. For this reason, the original gravity gradients in GRF firstly had to be transformed from GRF to Inertial

Reference Frame (IRF), then from IRF to Earth-Fixed Reference Frame (EFRF) and at last from EFRF to LNOF.

The transformation from GRF to IRF requires the creation of the rotation matrix $R_{IRF \to GRF}$, which uses the quaternions q1,q2,q3 and q4 of the GO_CONS_EGG_NOM_2 (.sgg) file (columns 56-59). These quaternions correspond to the rotation from IRF to GRF and the computation formula has the following form:

$$V_{IRF} = R_{IRF \to GRF}^T V_{GRF} R_{IRF \to GRF} \qquad (1.4.1)$$

The transformation from IRF to EFRF needs the computation of the rotation matrix $R_{EFRF \to IRF}$, which is created using the quaternions from the GO_CONS_SST_PSO_2 (.qat) file (columns 2-5). The quaternions in this file have to be interpolated in the GPS times of the EGG_NOM file as described in the GOCE Level 2 Product Data Handbook (ESA 2014). The rotation matrix refers to the transformation from EFRF to IRF and the transformed gradients in EFRF are thusly computed using the following equation:

$$V_{EFRF} = R_{EFRF \to IRF}^T V_{IRF} R_{EFRF \to IRF} \qquad (1.4.2)$$

The final step of the transformation procedure from EFRF to LNOF uses a rotation matrix ($R_{EFRF \to LNOF}$) that is computed by the longitude and latitude of the SST_PSO_2 file which have been interpolated with spline interpolation as described in section 1.3. Regarding the LNOF reference system, in GOCE standards, this is a North-West-Up reference system, even though it can take the form of a North-East-Up system with some modifications. In our case for the transformation of the original gradients from GRF to LNOF, the LNOF is defined as a North-East-up system. The following equation represents the computation of the transformed gravity gradients in LNOF:

$$V_{LNOF} = R_{EFRF \to LNOF} V_{EFRF} R_{EFRF \to LNOF}^T \qquad (1.4.3)$$

It is noting that the Vxy and Vyz gradients are being measured by an order of magnitude worse than the other four gradients, resulting in errors in the computation of all the six gradients in LNOF. Figure 1 that follows, presents the original GGs in GRF for one day of the satellite's measurements (1st January 2010), while the transformed GGs of the same day in IRF, EFRF and LNOF are presented in Figure 3 and **Figure 4** respectively. The introduction of errors in the Vxy and Vyz components can be clearly seen in the transformed GGs.

1.5   Filtering

GOCE Satellite Gravity Gradiometry (SGG) data are strongly correlated within the tensor components. Due to the gradiometer's design, the GOCE satellite can only achieve high accuracy and stable measurements in the measurement bandwidth (MBW), 0.005 Hz to 0.1 Hz. Outside of the MBW, noise with with sharp peaks is observed, especially in the frequencies lower than 0.005 Hz (Jarecki et al. 2006; Krasbutter et al. 2014; Wan, Yu, and Zeng 2012).

H.F.R.I.
Hellenic Foundation for
Research & Innovation

GeoGravGOCE

Ref: Con. Nr. 3488
Version: 1.0
Date: 1.21.2020
Page: 15/37
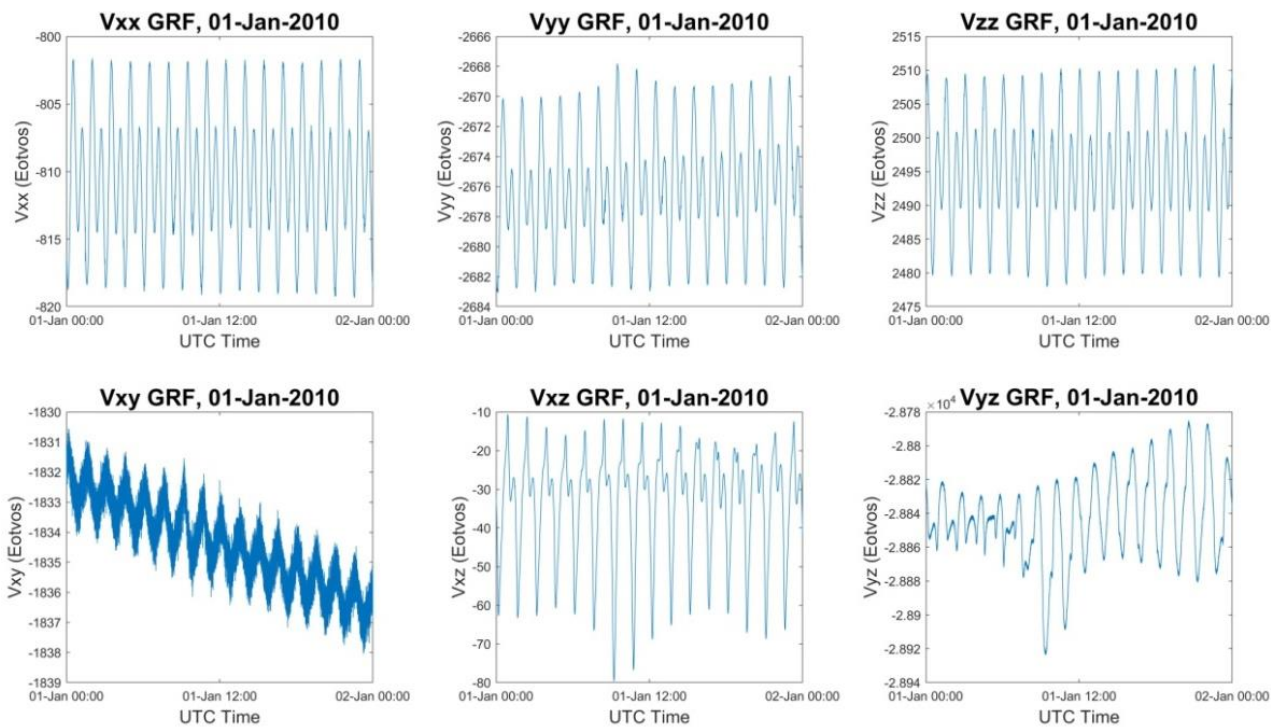
Figure 1: Gravity gradients in GRF
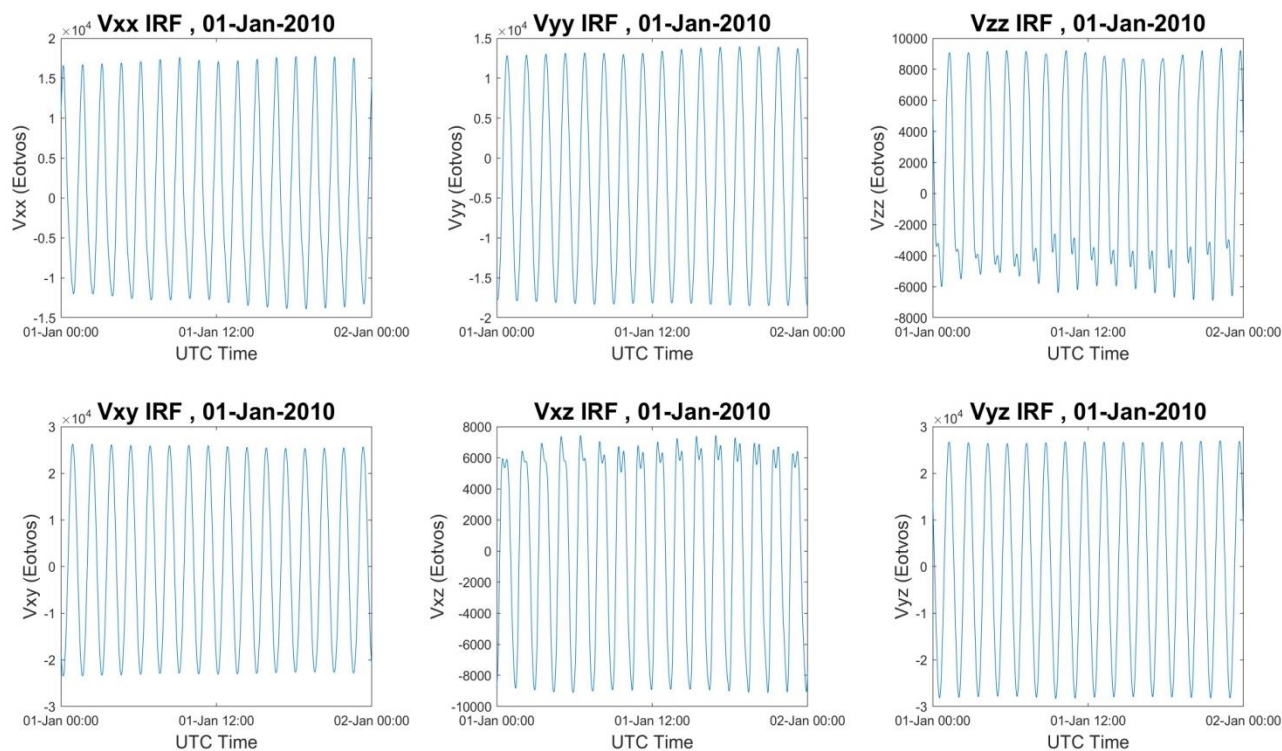
Figure 2: Gravity gradients in IRF

H.F.R.I.
Hellenic Foundation for
Research & Innovation

GeoGravGOCE
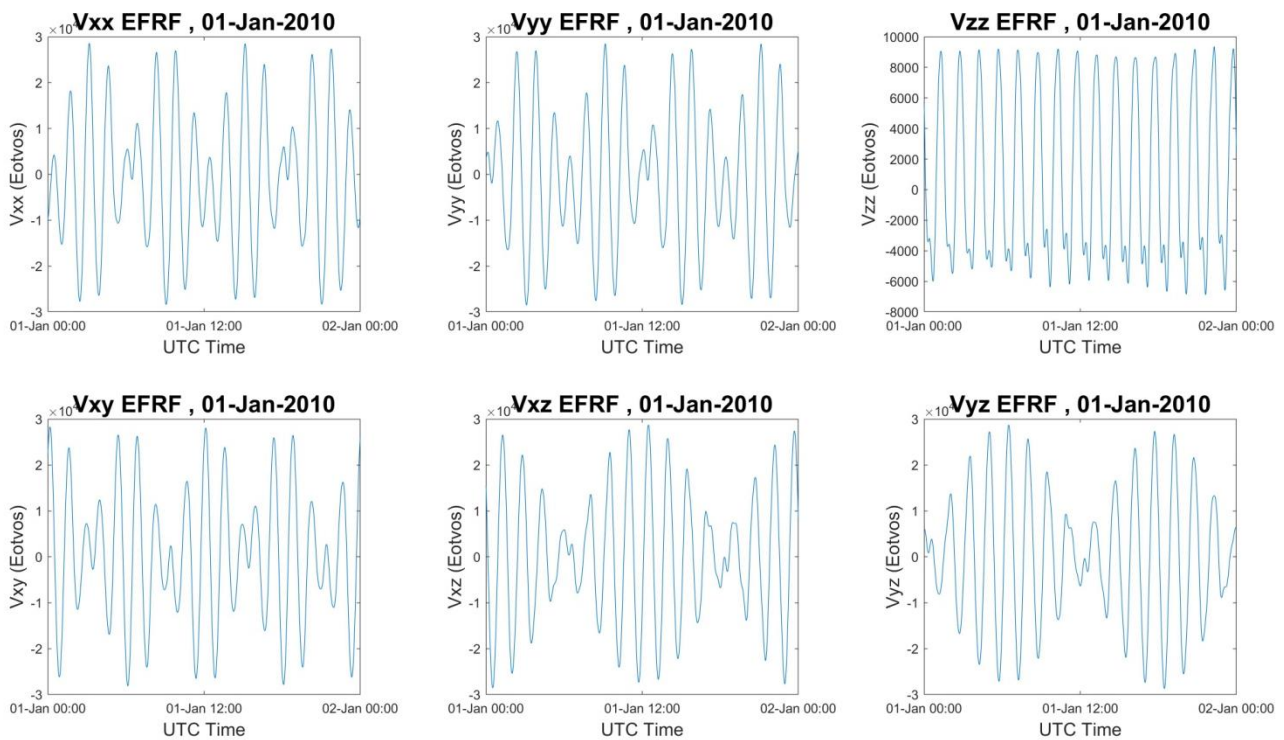
Figure 3: Gravity gradients in EFRF
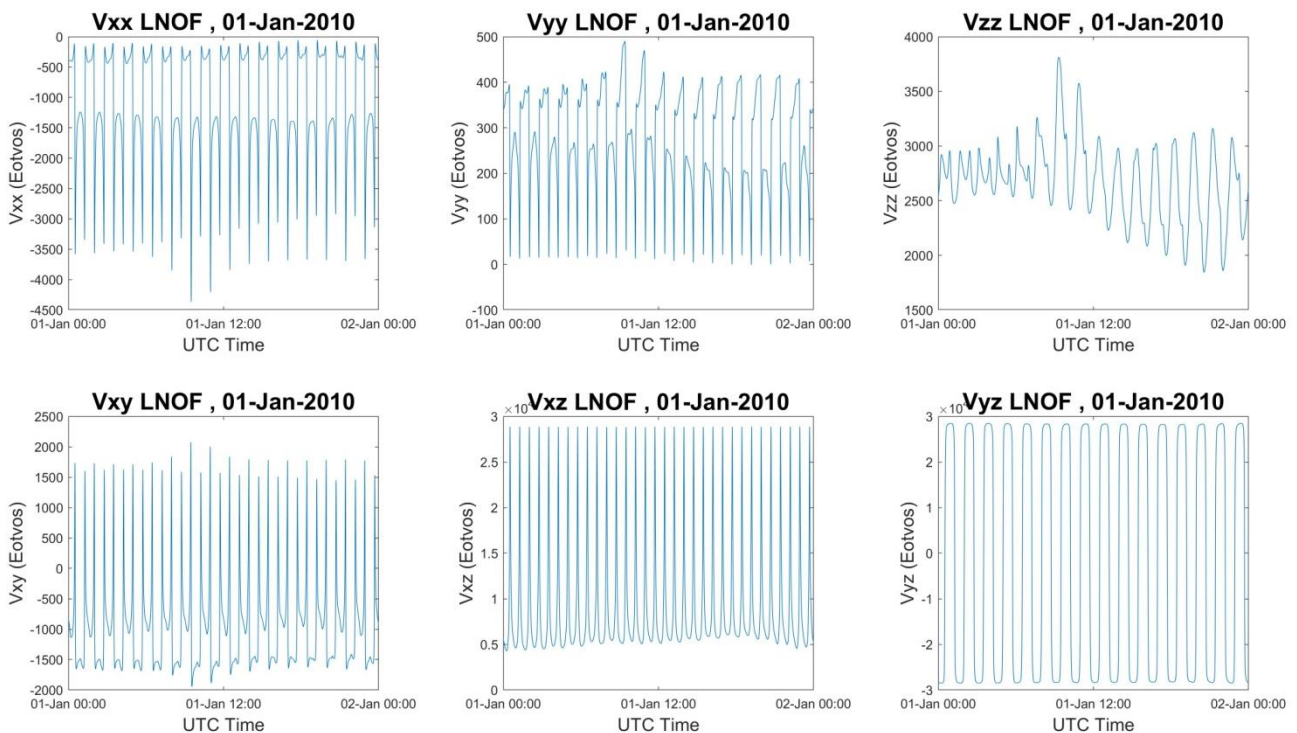
Figure 4: Gravity gradients in LNOF

In this section, the main objective is to investigate the proper filtering in order to process and remove those low-frequency (long-wavelength correlated) errors and get the GOCE signal with the highest possible quality. Three different spectral filters and their application to GOCE SGG data are introduced, in order to investigate the best filtering option. All types of filters were designed using the Matlab software (Matlab 2019b).

1.5.1 Finite Impulse Response (FIR) filter

The FIR filter is a non-recursive filter; this means that its output is computed by applying only the current and previous inputs. Therefore, there is no feedback in the filter structure, so it is always stable (Grout 2008). The filter's difference equation is presented in Equation 1.5.1 where $x(n)$ is the filter's input, $y(n)$ is the filter's output, $a(k)$ is the transfer function coefficients, N is the number of terms, known as filter's order and the first sample in the time is at $n = 0$.

$$y(n) = \sum_{k=0}^{N} a(k)x(n-k)$$

(1.5.1)

In this study, FIR is a bandpass filter that attenuates the signal outside of GOCE MBW, while the Hamming window is used to minimize the spectral leakage error in the boundaries of the determinate MBW.

Several filtering options were tested. The band-pass filter of FIR processed the testing SGG data, provided by ESA, from 1 to 31 January 2010, with 300, 500, 700, 1000, 1500, and 1700 orders (N). The SGG data on 1 January 2010 has been used for the filtering tests. Note that filtering was performed separately for each tensor component in the GRF. Indicatively, we in Figure 5 and Figure 6 the power spectral density (PSD) of the SGGs for the order 300 and 1500 for one day, is depicted respectively.

Figure 5: PSDs of unfiltered and FIR filtered tensor components, for order N=300.

Ref: Con. Nr. 3488
Version: 1.0
Date: 1.21.2020
Page: 18/37

H.F.R.I. Hellenic Foundation for Research & Innovation

GeoGravGOCE

Figure 6: PSDs of unfiltered and FIR filtered tensor components, for order N=1500.

In Figure 5 and Figure 6 the signals in the passbands appear to be stable after filtering while the GOCE signals seem to attenuate remarkably beyond the passband, especially as the order increases. Figure 5, Figure 7, Figure 8, and Figure 9 below represent the global maps of the unfiltered, and the FIR (N=1500) filtered SGG data in GRF, for January 2010. The zonal structure, which appears on the unfiltered data, is due to the satellite's orbit track. Note that the limits of the color bars are not the same as they differ on numerous orders of magnitude.
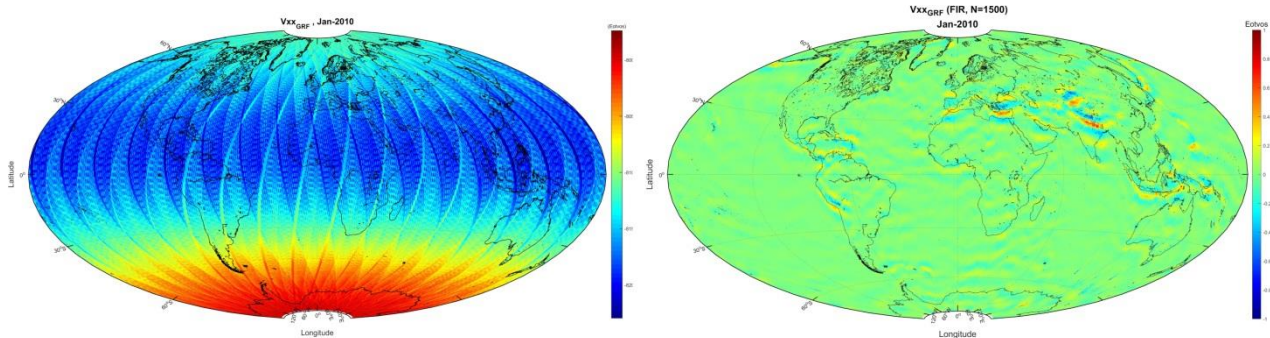
Figure 7: Unfiltered (left) and filtered (right) Vxx component in GRF
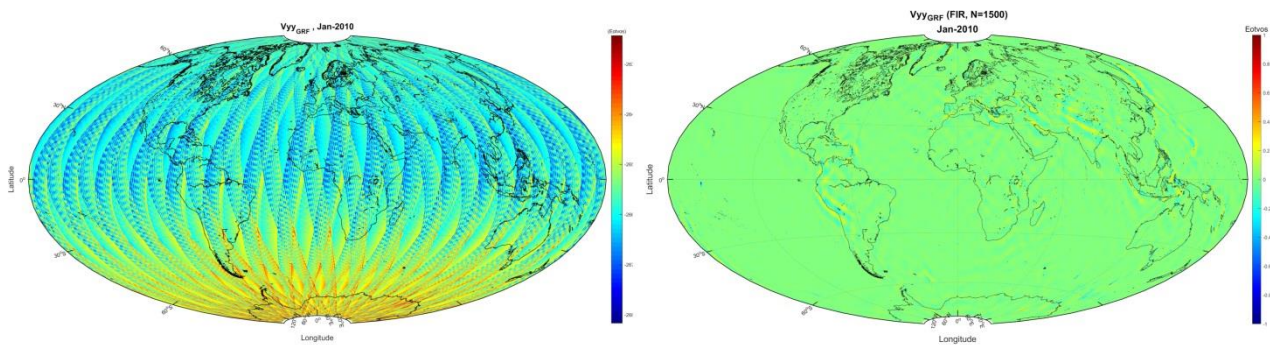
Figure 8: Unfiltered (left) and filtered (right) Vyy component in GRF
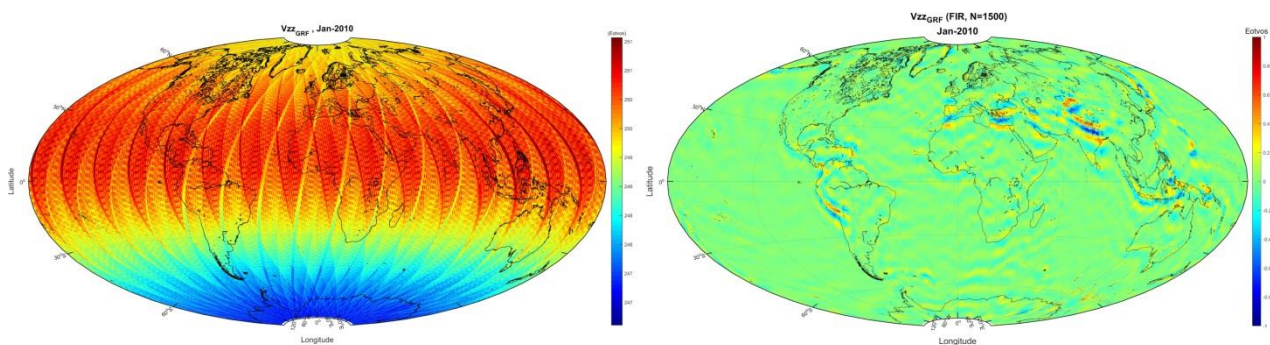
Figure 9: Unfiltered (left) and filtered (right) Vzz component in GRF

1.5.2   Infinite Impulse Response Filters (IIR) filter

The IIR is a recursive filter, in contradiction to FIR; this signifies that the filter's output is computed using the current and former inputs and former outputs (Grout 2008). In other words, it computes a weighted sum of input samples, precisely as the FIR filter's operation, and it adds to the actual amount a weighted sum of former output samples. The filter's difference equation is presented in Equation 1.5.1, where $x(n)$ is the filters' input, $y(n)$ is the filter's output, the $a(k)$ is the feedback coefficients, and $b(j)$ is the feed-forward coefficients. The N and M are the number of terms, known as filter's order while in order to compute each output signal value $(N\,M + 1)$ multiplies are required.

$$y(n) = \sum_{k=0}^{N} a(k)x(n-k) + \sum_{j=0}^{M} b(j)y(n-j) \qquad (1.5.2)$$

Multiple filtering experiments were also tested and for this case of filtering. SGG data for one month were tested for orders (N) 3, 5, and 7. Note that filtering was performed separately for each tensor component in the GRF. Indicatively, Figure 1 and Figure 2 depict the power spectral density (PSD) of the SGGs for the order 3 and 5 for one day, respectively.
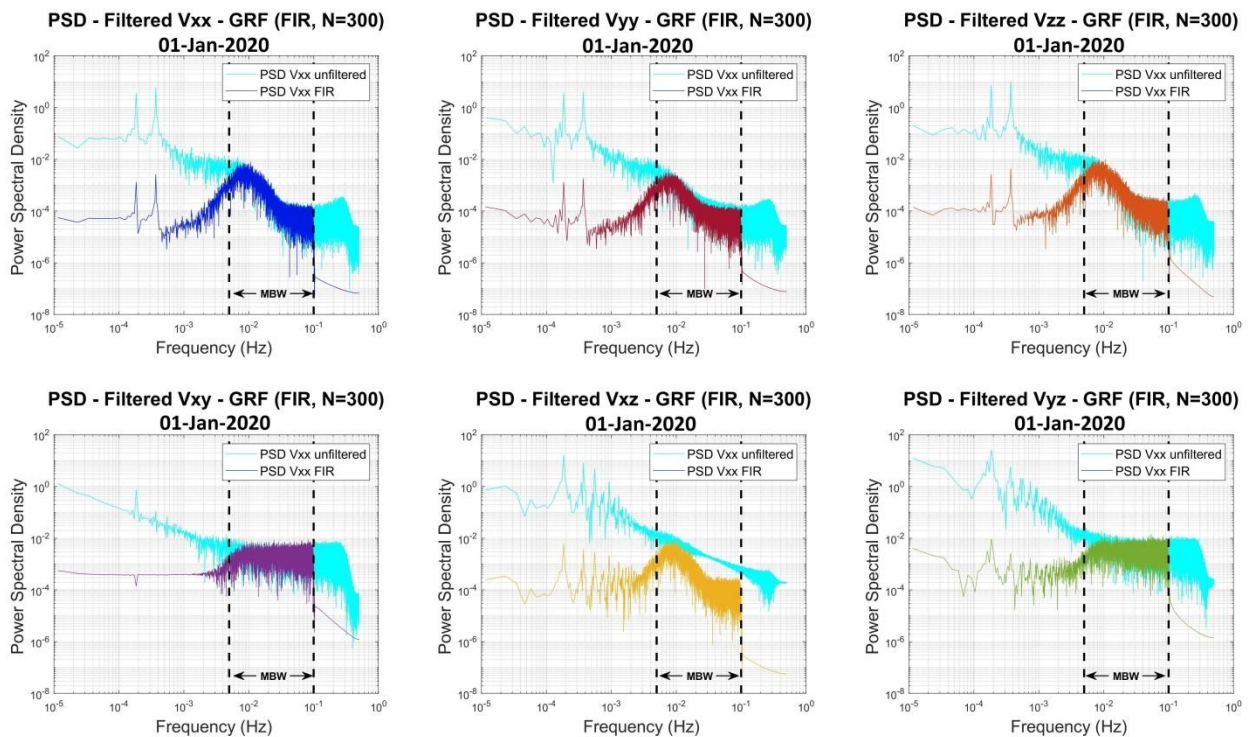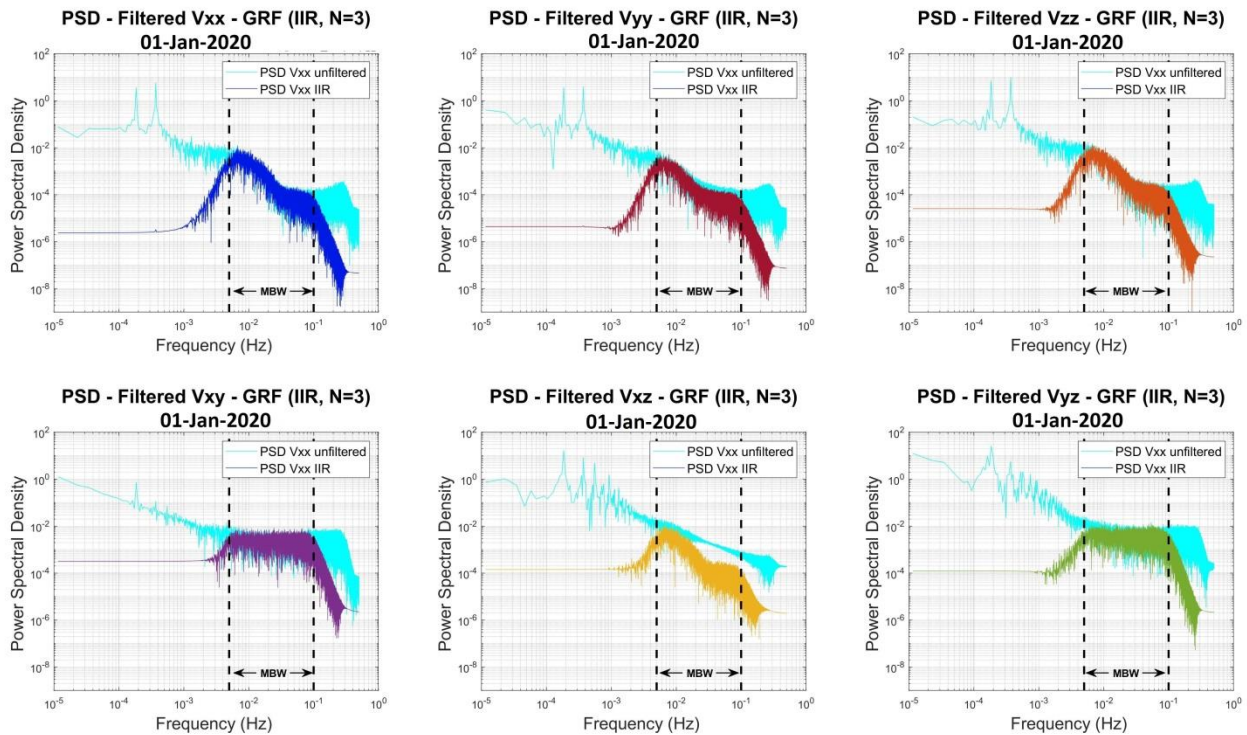
Figure 10: PSDs of unfiltered and IIR filtered tensor components, order N=3

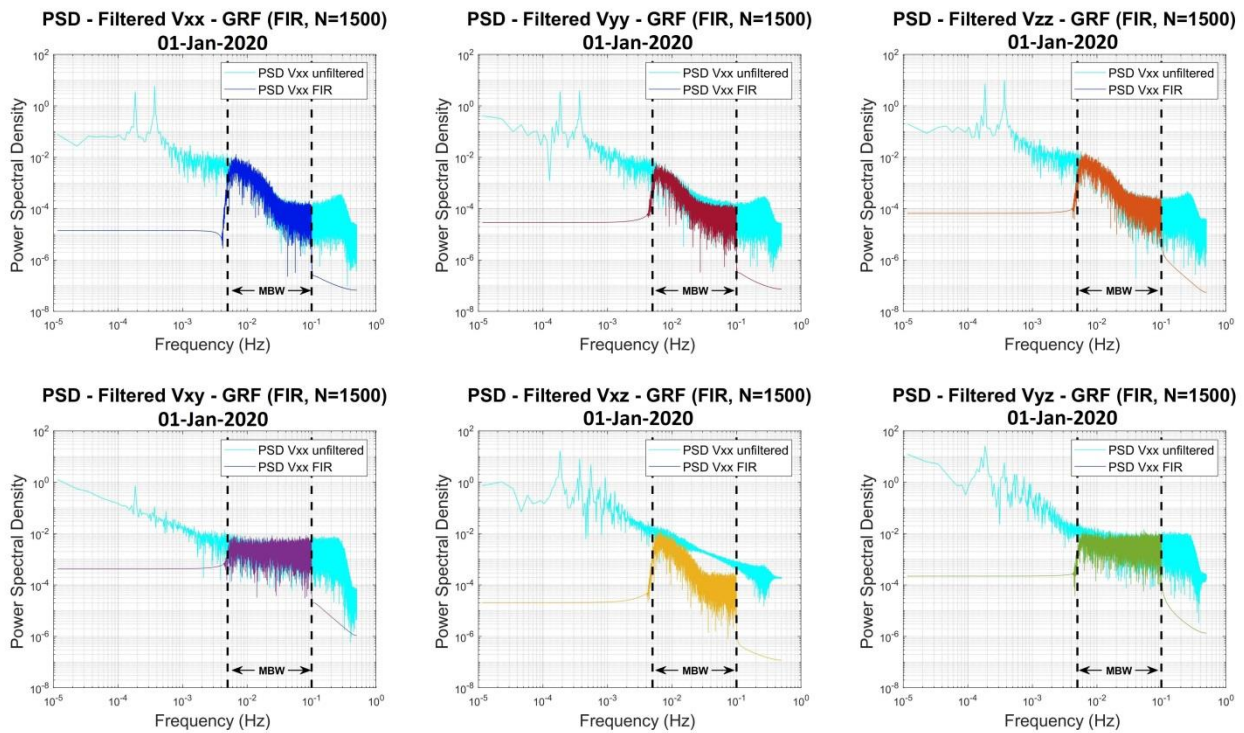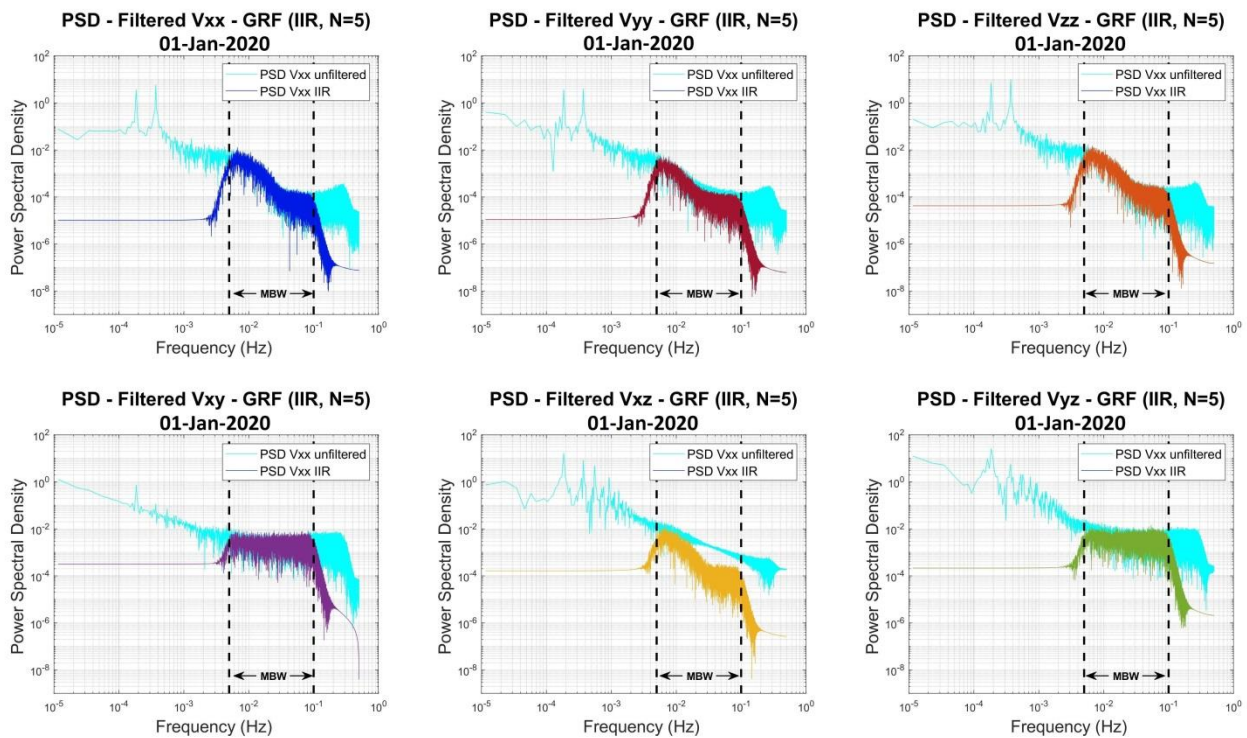**Figure 11:** PSDs of unfiltered and IIR filtered tensor components, order N=5

The figures above show that the filter can remove low-frequency errors while preserving pass-band signals. However, it seems that the filter doesn't respond precisely in the outside boundaries. The vertical dashed lines in the figures above designate the cut-off frequencies of the band-pass filters. The signal outside of MBW not only contains useful information for the SGGs but also includes noise

H.F.R.I.
Hellenic Foundation for
Research & Innovation

GeoGravGOCE

characteristics and further investigation needed. Figure 12, shows the global maps for January 2010 for Vxx, Vyy and Vzz components in GRF after IIR ($N = 5$) filtering.
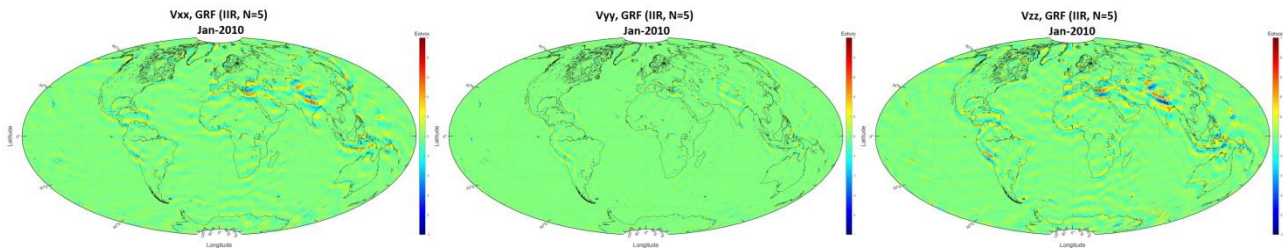
Figure 12: IIR (N=5), Filtered tensor components in GRF: Vxx (left), Vyy (middle) and Vzz (right).

The various FIR and IIR filter options tested show that both methods are efficient and simple, as the signals in the passband remain stable. The only disadvantage of the FIR filter is the significant number of orders required to implement it, as it requires more computation time and memory as a typical IIR filter has between 3-8 coefficients while the FIR filter maybe has over 500 coefficients.

1.5.3 *Wavelet MRA*

The last spectral filter tested was Wavelet (WL) Multi-Resolution Analysis (WL-MRA) (Mallat 1989). In this method, a Daubechies family wavelet (Daubechies 1992) with 10 vanishing moments (db10) at 12 levels of decomposition was applied along track (Grebenitcharsky and Moore 2014) in the original unfiltered gravity gradients in GRF. The signal of each gradient was decomposed at 12 levels with each level corresponding to a spatial resolution, with the first one extending from 8 to 16 km, the second one from 16 to 32 km etc. Every level of decomposition consists of a detail and an approximation coefficient. The power spectral density (PSD) of each coefficient was computed in order to determine which levels carry useful information inside the Measurement Bandwidth (MBW) of the GOCE satellite, with the detail coefficients of levels 3 to 7 mainly identified as such. In particular the third level carried information both inside and outside of the MBW. The decomposed signal can be reconstructed by summing the detail coefficients of each level and the approximation coefficient of the last level of decomposition, as shown in the following equation:

$$\text{s} = (\text{d}_1) + (\text{d}_2) + \ldots + (\text{a}_n + \text{d}_n) \tag{1.5.3}$$

Various reconstructions were applied according to the PSD of each coefficient, e.g., a synthesis using only the detail coefficients of levels 4 to 8, one that uses the detail coefficients of levels 4 to 8 and the approximation coefficient of the last level etc. Furthermore, the case of decomposing the signal at 14 levels and reconstructing at various scenarios was also tested. The final reconstruction selected was the one that used only the detail coefficients of levels 4 to 7 (at 12 levels of decomposition), corresponding to a scale from 64 to 1024 km.

Figure 13 presents the power spectral density of the reconstructed (l4..l7) V_{xx} gradient of the first orbit of the satellite in GRF at 01 January 2010. It can be seen that the biggest part of useful information of our reconstructed signal is inside the MBW of the satellite, meaning that noise from the lower and higher frequencies outside the MBW is being removed. The same behaviour was observed also in the remaining five gradients (not shown here). Moreover, the monthly solutions of the synthesized (l4..l7) diagonal components of the gradient tensor (V_{xx}, V_{yy}, V_{zz}) are depicted in

Figure 14. Of interest are the observed values of the V_{xx}, V_{zz} gradients in areas like the Himalayas, Andes and the Mediterranean Sea.
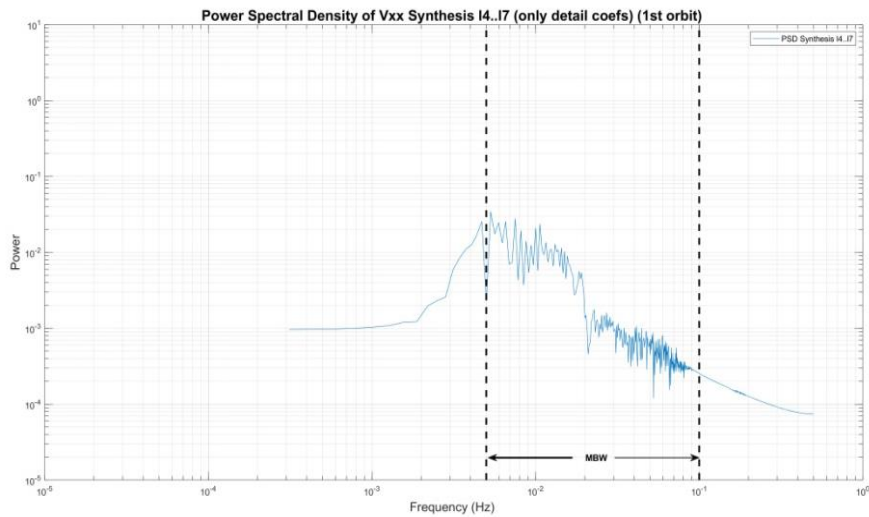

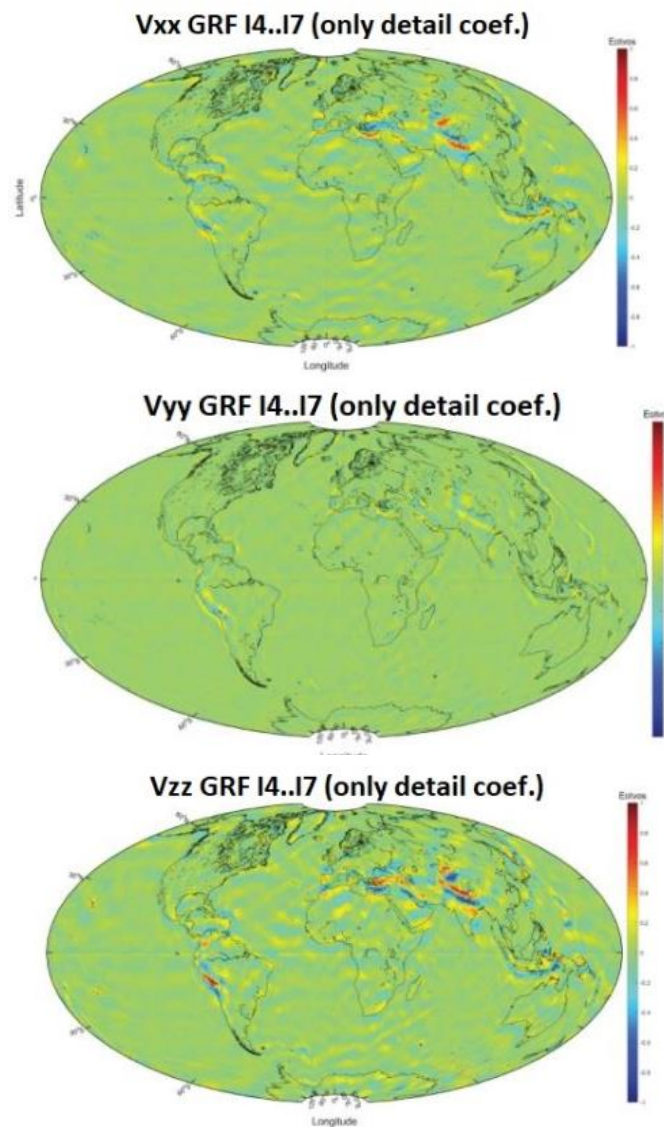Figure 13: Psd of V_{xx} synthesis(l4..l7) of the 1st orbit (01-Jan-2010).

Figure 14: Monthly V_{xx}, V_{yy}, V_{zz} synthesis (l4..l7), January 2010.

1.6   GrafLab GGM estimation

After the pre-processing of the GOCE SGG data, the gravitational tensors in the LNOF were computed, for each file, using GrafLab (2.1.4). Several tests of GGM synthesis has been performed in order to choose the proper model for further calculations. Three different geopotential models were downloaded from the International Centre for Global Earth Models (ICGEM) and tested in order to choose the proper one.

GO_CONS_GCF_2_TIM_R6 complete to degree and order 240 and 300, GOCO06s complete to degree and order 240 and 300, and finally, and XGM2019e_2159 complete to degree and order 2190 were the options tested. For the computation of the gravitational tensors, in GrafLab's environment, the same parameters were used, for the reference ellipsoid and the radius of the geopotential model. In Table 1, the mean value of the gravitational tensor components in LNOF is presented, which is the actual output of GrafLab, of all the GGMs which computed.

Table 1: Mean Value of GrafLab's models, in LNOF (Eotvos).

		TIM_R6-240	TIM_R6-300	GOCO06s_240	GOCO06s_300	XGM_2190
mean	Vxx	270047.5223	270047.5223	270047.5223	270047.5223	270047.5223
	Vyy	-1362.0870	-1362.0870	-1362.0870	-1362.0870	-1362.0870
	Vzz	-1360.0188	-1360.0188	-1360.0188	-1360.0188	-1360.0188
	Vxy	2722.1058	2722.1058	2722.1058	2722.1058	2722.1058
	Vxz	0.0005	0.0005	0.0005	0.0005	0.0005
	Vyz	0.0257	0.0257	0.0257	0.0257	0.0257

The mean value of all models are equal, so the TIM R6 model with degree 300, being a GOCE-only satellite models, is chosen for the following experiments of the GOCE data reduction.

1.6.1   Transformed GGM estimation

The GrafLab exported GGM gravity gradients refer to the LNOF (Local North-West-Up, therefore the transformation from LNOF to GRF is needed in order to process them with the initial SGGs in the same reference system. This includes the transformation first from LNOF to EFRF, then from EFRF to IRF, and finally from IRF to GRF. Similarly to the transformation from GRF to LNOF, described in section 1.4, the inverse transformation is described by a series of equations modified for the inverse procedure:

$$V_{EFRF} = R^T_{EFRF \rightarrow LNOF} V_{LNOF} R_{EFRF \rightarrow LNOF} \tag{1.6.1}$$

$$V_{IRF} = R_{EFRF \rightarrow IRF} V_{EFRF} R^T_{EFRF \rightarrow IRF} \tag{1.6.2}$$

$$V_{GRF} = R_{IRF \rightarrow GRF} V_{IRF} R^T_{IRF \rightarrow GRF} \tag{1.6.3}$$

In Figure 15 the GGM-derived gravity gradients in the LNOF, for this case of TIM release 06 (TIM R6) up to degree and order 300 (d/o:300), for one day (1st January 2010) are presented, while in Figure 16, Figure 17 and Figure 18 the transformed gradients in EFRF,IRF and GRF are depicted. It has to be pointed out that many experimental scenarios concerning different geopotential models and their transformations from LNOF to GRF have been taken out during this study. The mean values of each gradient component, in this case, in the four reference systems (LNOF, EFRF, IRF and GRF) are respectively shown in Table 2, Table 3, Table 4 and Table 5.
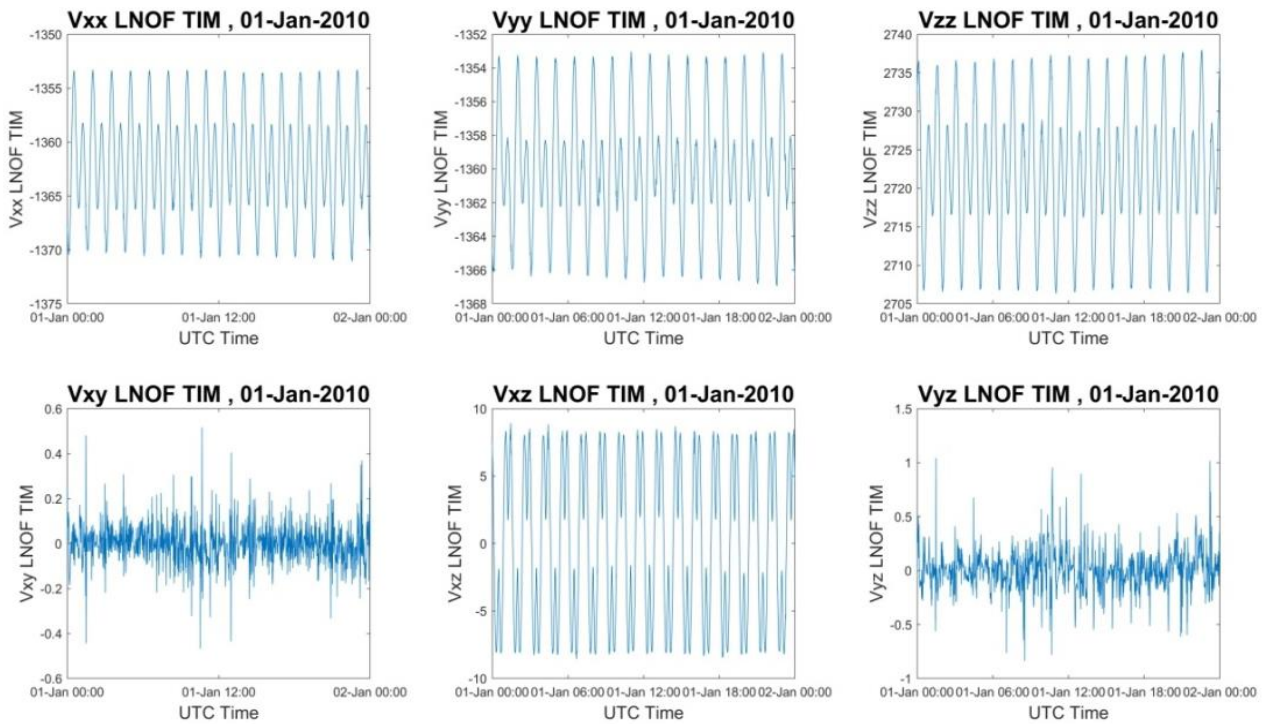
Figure 15: Gravity gradients of GGM in the LNOF

Table 2: Statistics of GGM's GGs in LNOF

LNOF (Eotvos)	Vxx	Vyy	Vzz	Vxy	Vxz	Vyz
Mean	-1362.087	-1360.019	2722.106	0.000	0.026	0.008
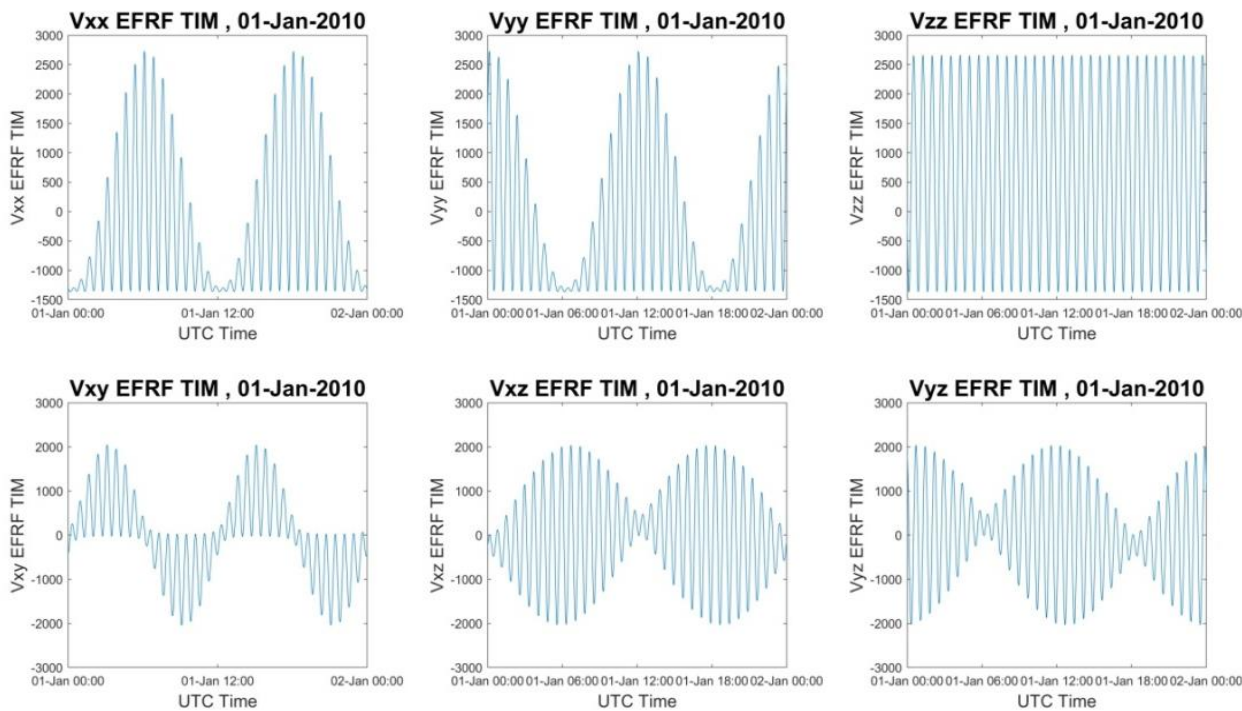
Figure 16: Gravity gradients of GGM in EFRF

Table 3: Statistics of GGM's GGs in EFRF

EFRF (Eotvos)	Vxx	Vyy	Vzz	Vxy	Vxz	Vyz
Mean	-328.524	-324.546	653.070	-0.247	-1.322	6.780
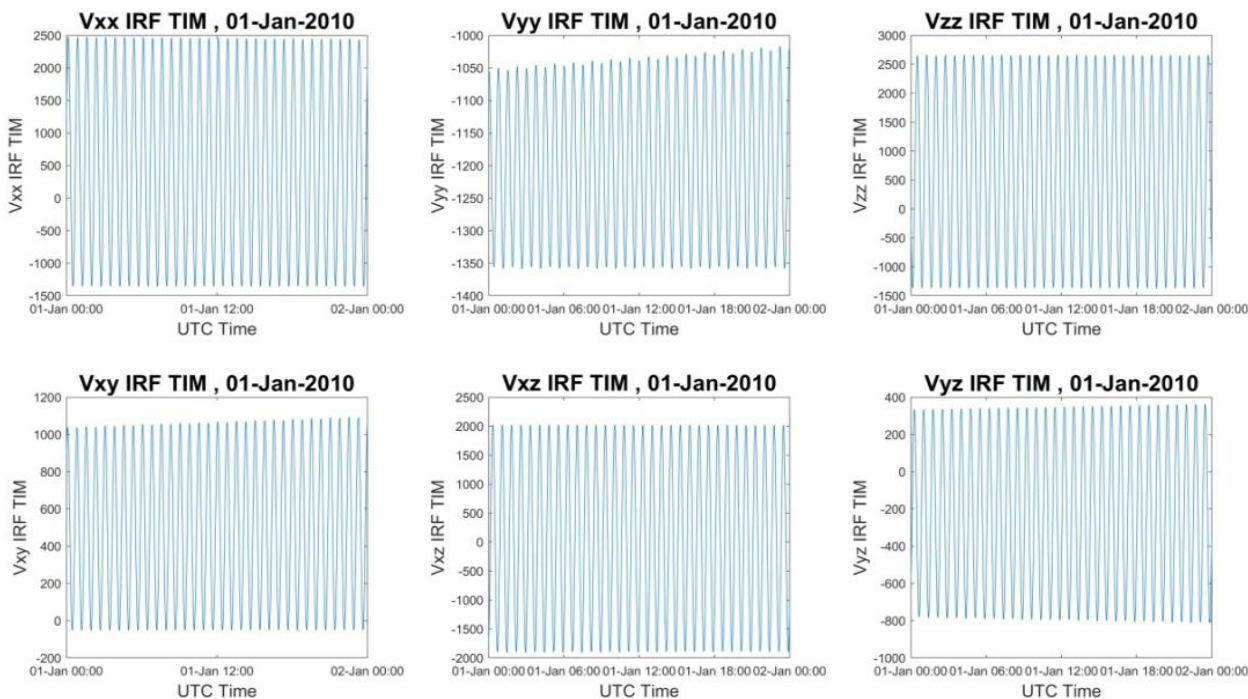
Figure 17: Gravity gradients of GGM in IRF

H.F.R.I.
Hellenic Foundation for Research & Innovation

GeoGravGOCE

Table 4: Statistics of GGM's GGs in IRF

IRF (Eotvos)	Vxx	Vyy	Vzz	Vxy	Vxz	Vyz
Mean	543.835	-1196.795	652.959	505.727	58.112	-225.603
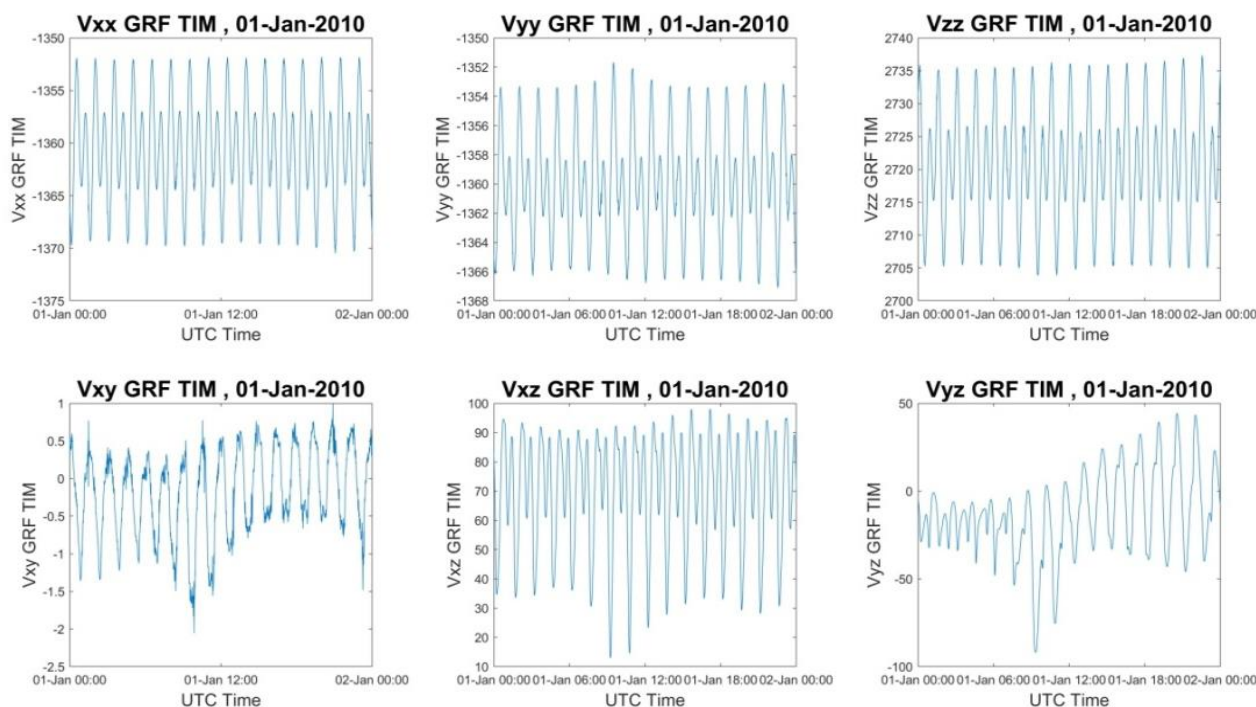
Figure 18: Gravity gradients of GGM in GRF

Table 5: Statistics of GGM's GGs in GRF

GRF (Eotvos)	Vxx	Vyy	Vzz	Vxy	Vxz	Vyz
Mean	-1360.714	-1359.927	2720.641	-0.172	69.826	-12.883

1.7 Data reduction and selective filtering

From the initial GOCE SGGs, the TIM R6 contribution in the GRF is removed. Note that, only for the V_{yz} component, due to the lower initial accuracy, its average value has been subtracted, as shown in Table 6. After the data is reduced, the filtering process is repeated.

Table 6: Statistics of Vyz component in GRF

Vyz (Eotvos)				
	Vyz (initial)	TIM 600	Vyz - mean(Vyz)	Vyz - mean(Vyz)-TIM600
min	-28924	-91.9278	-81.0941	-1.9472
max	-28785	44.2962	57.7861	26.0629
mean	-28843	-12.8832	0.0000	12.8832
std	25.0296	24.2754	25.0296	5.7192
RMS	28843	27.4821	25.0294	14.0956

Below, in Figure 19 and Table 7, the PSDs and the statistics of the reduced data in GRF for one day, are presented respectively.
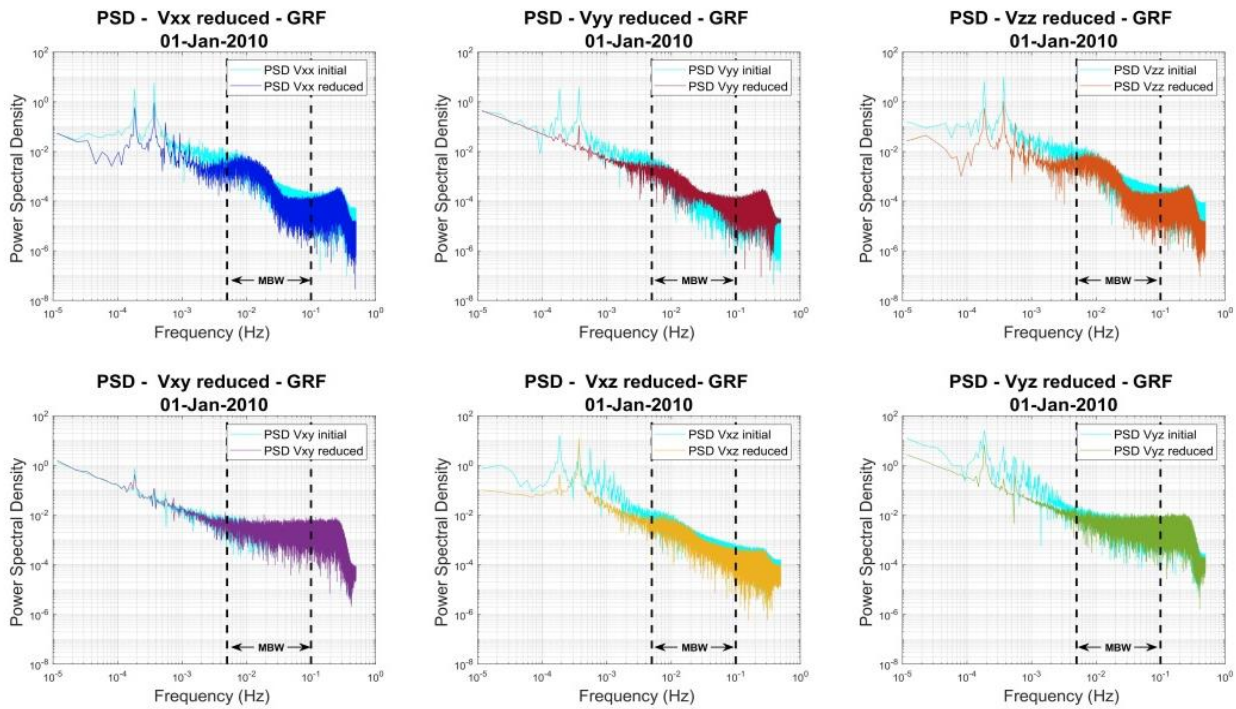
Figure 19: PSDs of reduced data in GRF

Table 7: Statistics of reduced data in GRF

Reduced data / GRF (Eotvos)							
		Vxx	Vyy	Vzz	Vxy	Vxz	Vyz*
01-Jan	min	548.6904	-1317.0158	-227.8811	-1837.9360	-117.1388	-1.8677
	max	552.3203	-1315.2251	-223.8419	-1830.9085	-90.4074	25.9651
	mean	550.2488	-1316.1333	-225.7298	-1834.2047	-103.4842	12.8827
	std	0.8035	0.4165	0.8711	1.4570	9.0641	5.6672
	RMS	550.2493	1316.1334	225.7315	1834.2053	103.8804	14.0742

1.7.1   FIR 1500

After several experiments on FIR filters, it was found out that the FIR 1500 corresponds optimally in the filtering requirements. Figure 20 and Table 8 present the PSDs and the statistics of the reduced data in GRF for one day while Figure 24 and Table 9 display the corresponding PSDs and the statistics of the reduced data in GRF for one month.

Figure 20: PSDs of reduced filtered data in GRF

Table 8: Statistics of FIR filtered data in GRF, for 1 January 2010.

FIR 1500 - Reduced data / GRF (Eotvos)							
		Vxx	Vyy	Vzz	Vxy	Vxz	Vyz
01-Jan	min	-0.6855	-0.1973	-0.7370	-0.7133	-0.7523	-1.1485
	max	0.5892	0.2553	0.8352	0.7130	0.8304	1.0427
	mean	0.0000	0.0000	0.0000	-0.0002	0.0000	0.0000
	std	0.0628	0.0235	0.0785	0.1787	0.0726	0.2664
	RMS	0.0628	0.0235	0.0785	0.1787	0.0726	0.2664
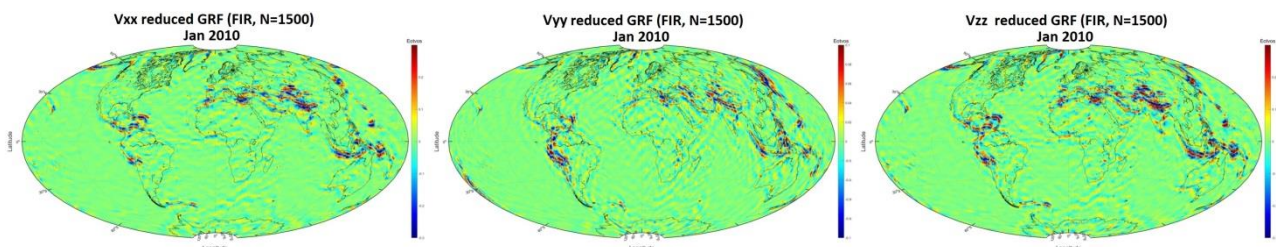
Figure 21: Reduced filtered data in GRF for January 2010: Vxx (left), Vyy (middle) and Vzz (right)

Table 9: Statistics of FIR filtered data in GRF, for 1 month (Eotvos)

Component	min	max	mean	std	rms
Vxx	-0.83452	1.23672	0.00001	0.06405	0.06405
Vyy	-0.29993	0.31229	-0.00002	0.02249	0.02249
Vzz	-1.34752	1.12145	-0.00001	0.07862	0.07862

1.7.2 IIR 5

After various tests on IIR filters, it was found out that the IIR 5 corresponds optimally in this project's filtering requirements. Figure 22 and Table 10 present for one day, the PSDs and the statistics of reduced filtered data in GRF for one day, while Figure 26 and Table 11 display the corresponding PSDs and the statistics of the reduced data in GRF for one month.
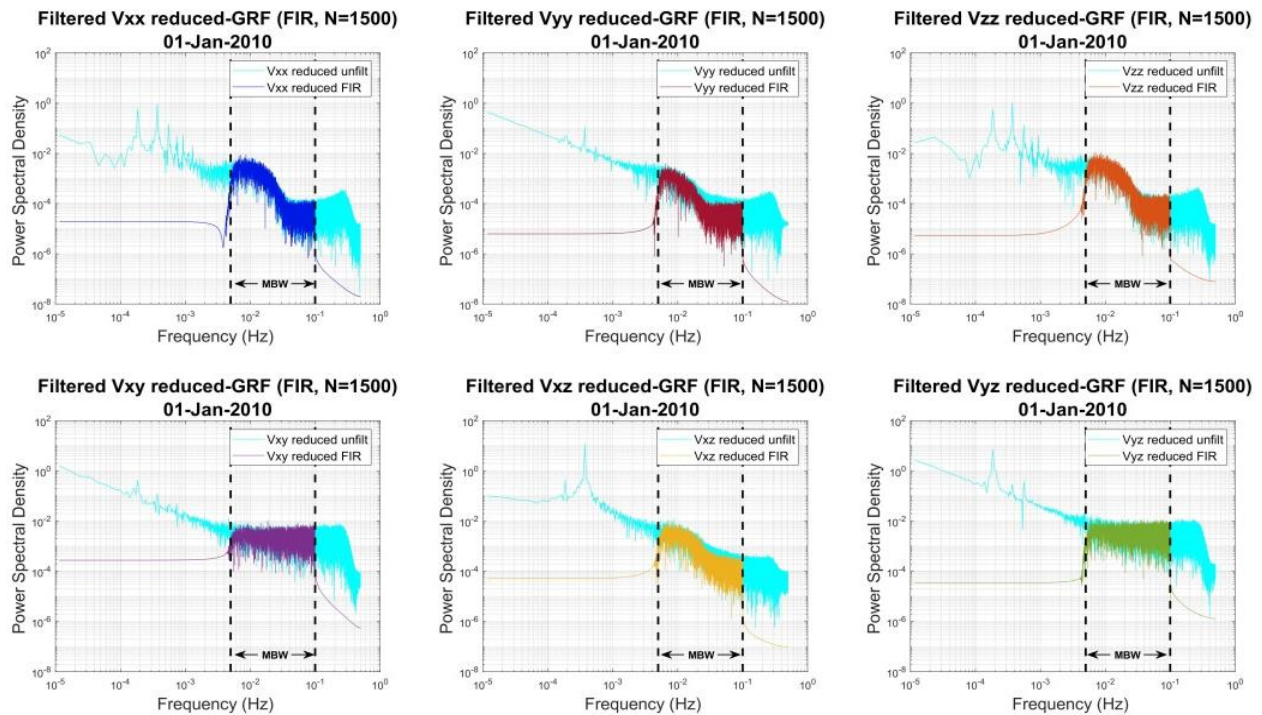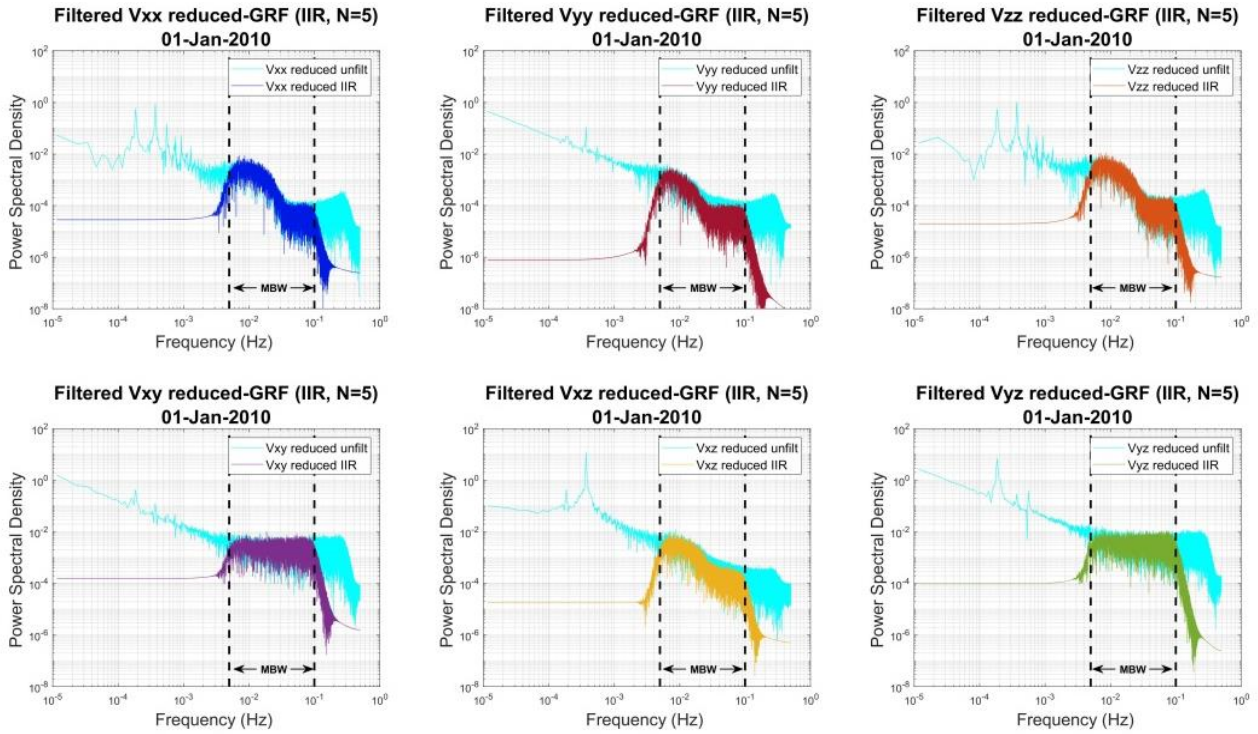

Figure 22: PSDs of reduced filtered data in GRF

Table 10: Statistics of IIR filtered reduced data in GRF

| IIR 5 - Reduced data / GRF (Eotvos)						
		Vxx	Vyy	Vzz	Vxy	Vxz	Vyz
01-Jan	min	-0.6914	-0.2009	-0.7424	-0.6837	-0.7427	-1.1694
	max	0.5891	0.2622	0.8335	0.6948	0.8177	1.0350
	mean	0.0000	0.0000	0.0000	-0.0001	0.0000	0.0000
	std	0.0626	0.0234	0.0782	0.1723	0.0723	0.2574
	RMS	0.0626	0.0234	0.0782	0.1723	0.0723	0.2574

Figure 23: Reduced filtered data in GRF for January 2010: Vxx (left), Vyy (middle) and Vzz (right)

Table 11: Statistics of FIR filtered data in GRF, for 1 month (Eötvös)

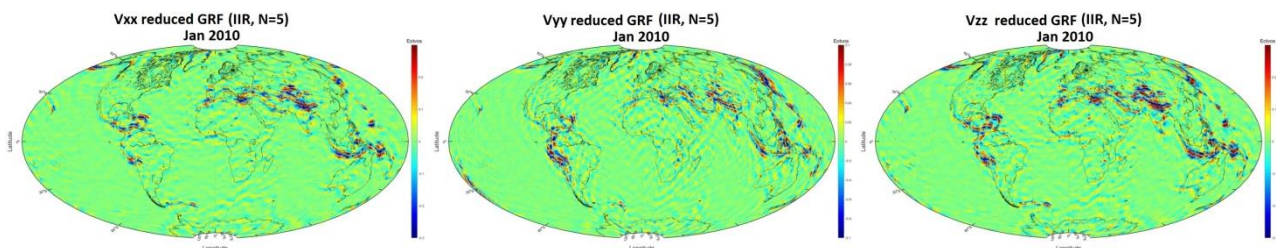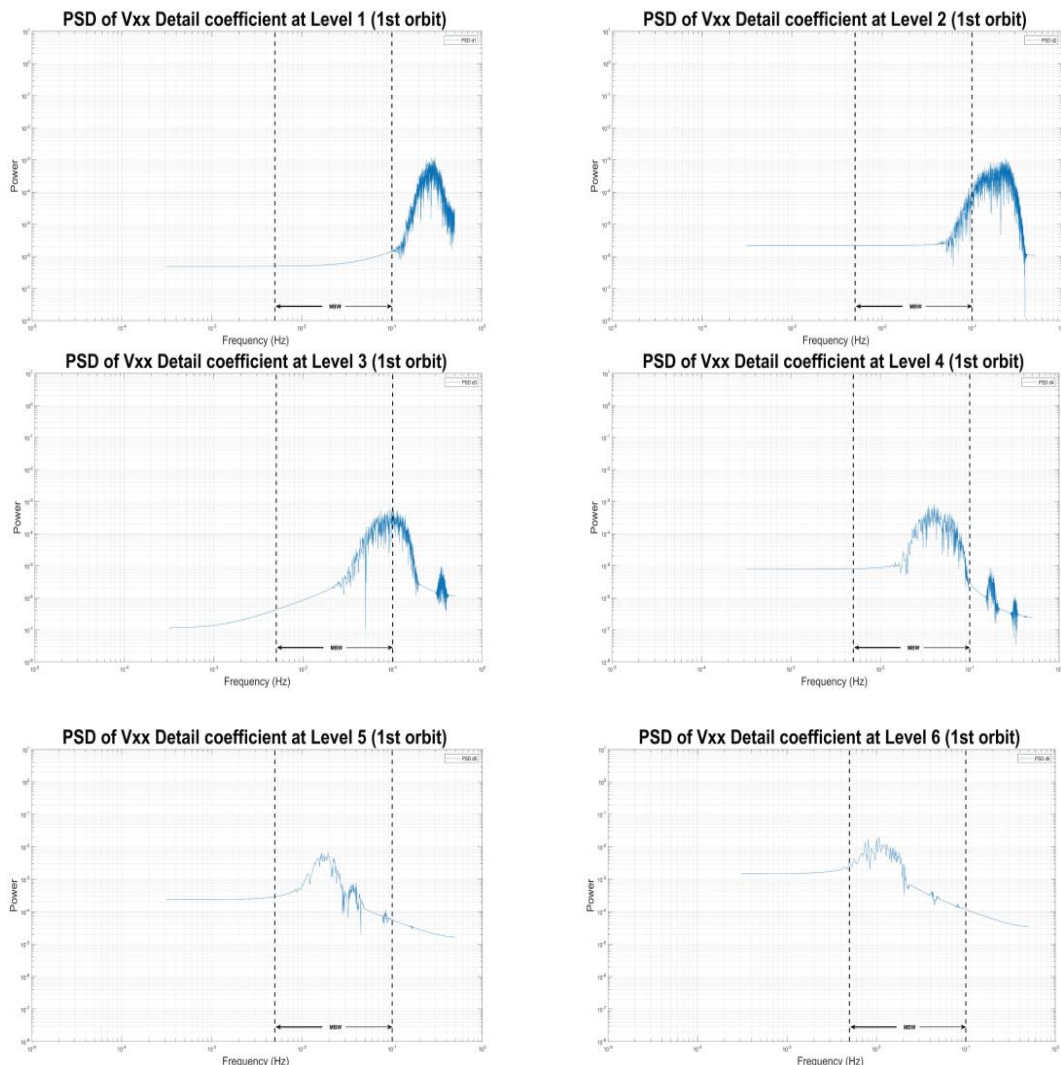| Component	min	max	mean	std	rms
Vxx	-0.84918	1.25024	0.00000	0.06384	0.06384
Vyy	-0.30636	0.31156	0.00000	0.02245	0.02245
Vzz	-1.36672	1.14303	0.00000	0.07837	0.07837

1.7.3   Wavelet MRA

A Wavelet Multi-Resolution Analysis was then applied to the reduced gravity gradients in GRF, in a similar way as in section. In Figure 24 the PSDs of the detail coefficients of the reduced V_{xx} gradient for the first of 01 January 2010 can be seen. Inside the MBW mainly the PSDs of the detail coefficients of levels 3 to 7 are present. The Power Spectrum Density of various reconstruction scenarios of the V_{xx} component along with the initial reduced signal for one day of data (01 January 2010) is presented in Figure 25, while Figure 26 exhibits the same kind of information but this time for data of one month (January 2010). In general, it can be stated that the reconstructed signals containing the approximation coefficient of the last level of decomposition were heavily influenced by noise. As a result, in most scenarios, this coefficient was omitted from the reconstructions, which were mainly containing the detail coefficients whose PSDs were inside the upper and lower limits of the MBW. Finally, Figure 27 contains the monthly solutions of January 2010 for the (l4..l7) reconstructed V_{xx}, V_{yy} and V_{zz}.

H.F.R.I.
Hellenic Foundation for
Research & Innovation

GeoGravGOCE

Ref: Con. Nr. 3488
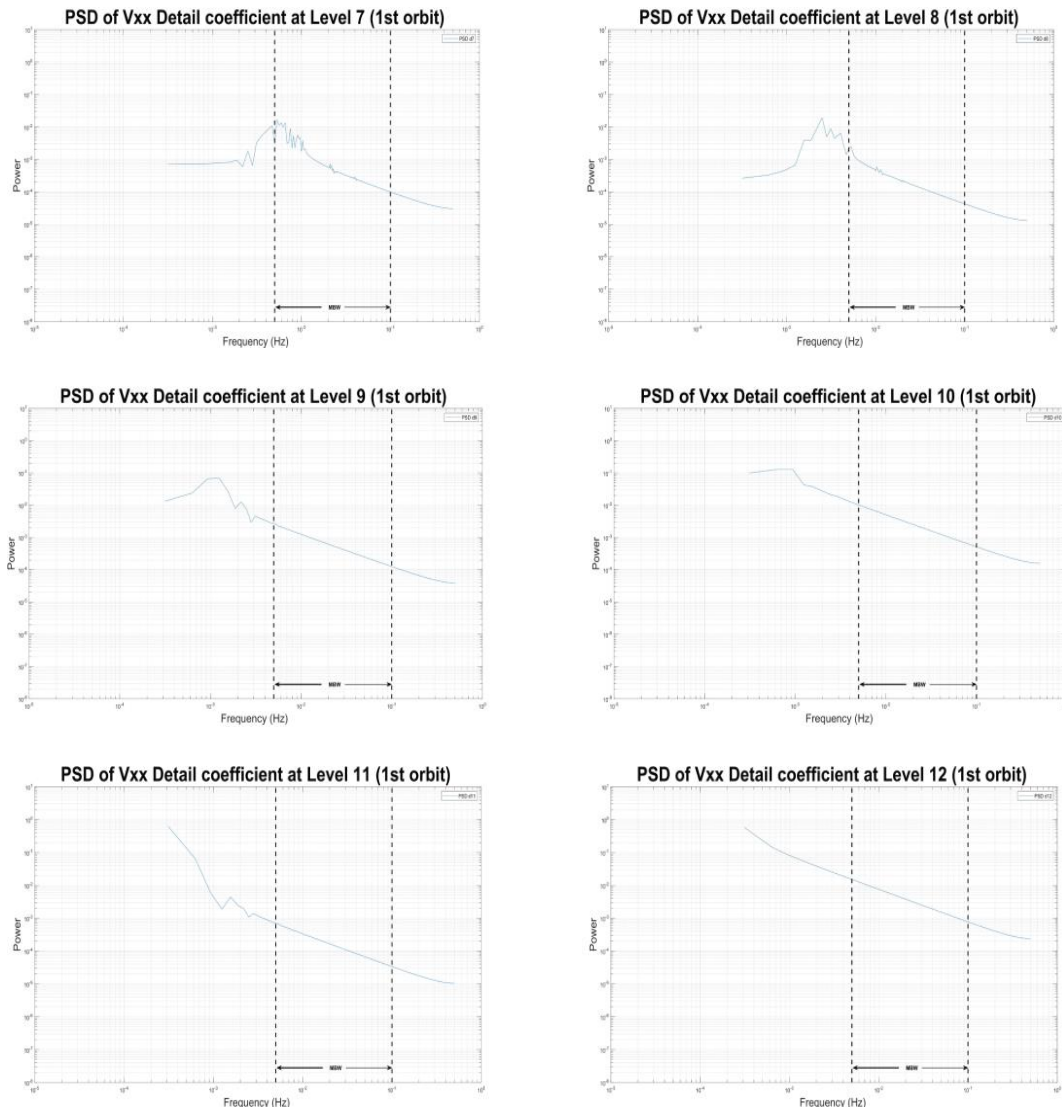Version: 1.0
Date: 1.21.2020
Page: 31/37

Figure 24: PSDs of the detail coefficients of the reduced V_{xx} gradients (1st orbit - 01-Jan-2010)
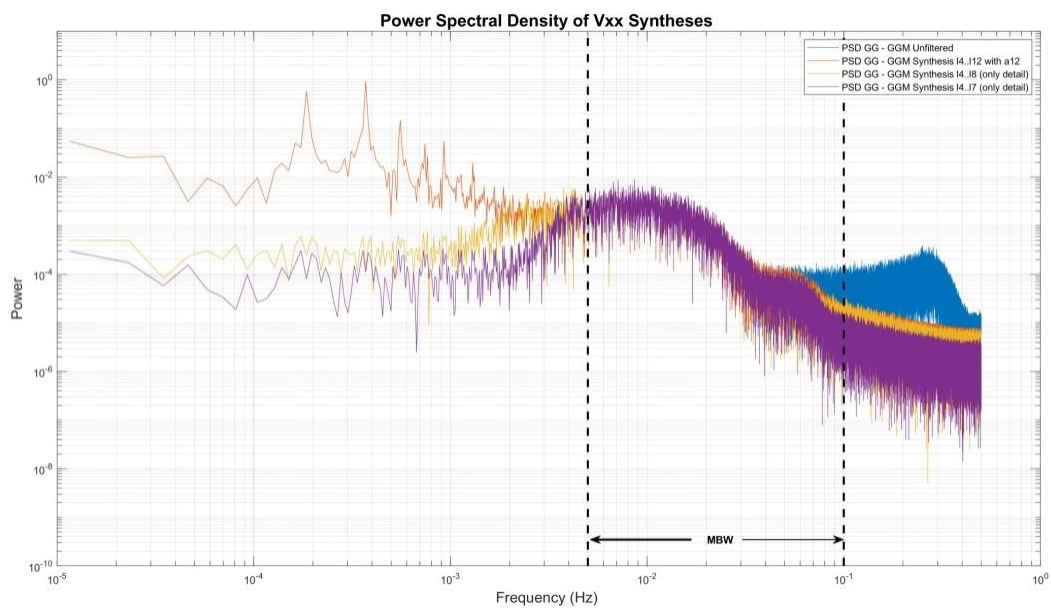
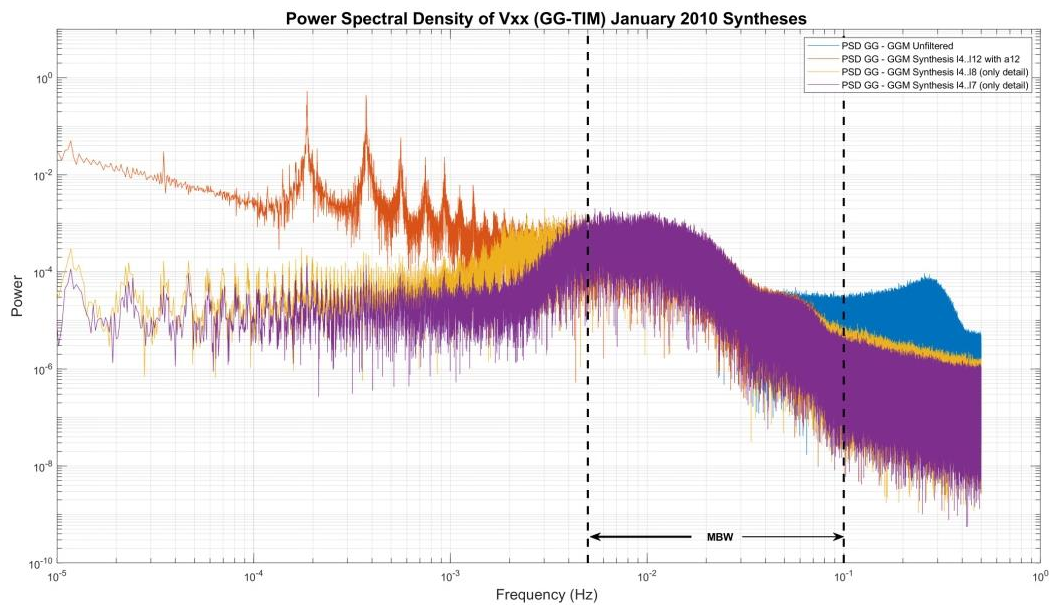**Figure 25:** PSDs of various cases of syntheses of the reduced V_{xx} gradient for one day (01-Jan-2010)

H.F.R.I.
Hellenic Foundation for
Research & Innovation

GeoGravGOCE

Figure 26: PSDs of various cases of syntheses of the reduced V_{xx} gradient for one month (January 2010)
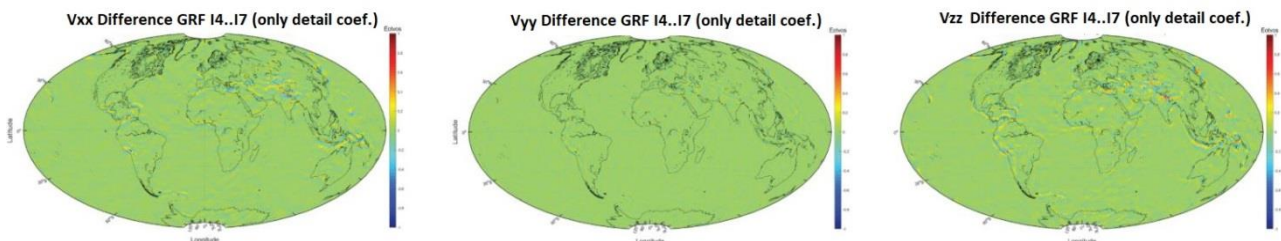

Figure 27: Monthly reduced V_{xx}, V_{yy} and V_{zz} synthesis(l4..l7) in GRF, January 2010

Table 12: Statistics of Wavelet (l4..l7) filtered data in GRF, for 1 month (Eötvös)

Component	min	max	mean	std	rms
Vxx	-0.976	1.331	0.000	0.068	0.068
Vyy	-0.830	1.196	0.000	0.026	0.026
Vzz	-1.471	1.317	0.000	0.085	0.085

1.8 Development of the GeoGracGOCE software GUI platform

One of the principal objectives of the GeoGravGOCE project is to develop a Graphical User Interface (GUI) for the developed software. The goal is to design a friendly, interactive, and serviceable GUI for the user. The software of Matlab and the App designer are used for the designing and building of the GUI. At this moment, the GUI has two functional tabs and one more tab is in progress. Various trials, experiments, and new methods of computations are performed to make it as efficient as possible.

The first tab of GUI refers to the pre-process of GOCE data. The main operation is the reading of the EGG_NOM_2 and PSO_2 data while the input data can be more than in one each time. Then the NOM data are compared and adjusted according to the length of PSO data. Also, the (X, Y, Z) coordinates in EFRF are interpolated and the geodetic coordinates $(lon, lat, altitude)$ in GRS80 are

H.F.R.I.
Hellenic Foundation for Research & Innovation

GeoGravGOCE

calculated. Following the end of this processing, the user has some options to choose from. For instance, the GUI provides statistics and graphs of the computed data. It also gives the opportunity to export the data in Graflab's format and the execution of the GrafLab directly. The only condition is that the user should have the *.m file of GrafLab already. The first tab named Calculate V_{ij} is shown below in Figure 28.
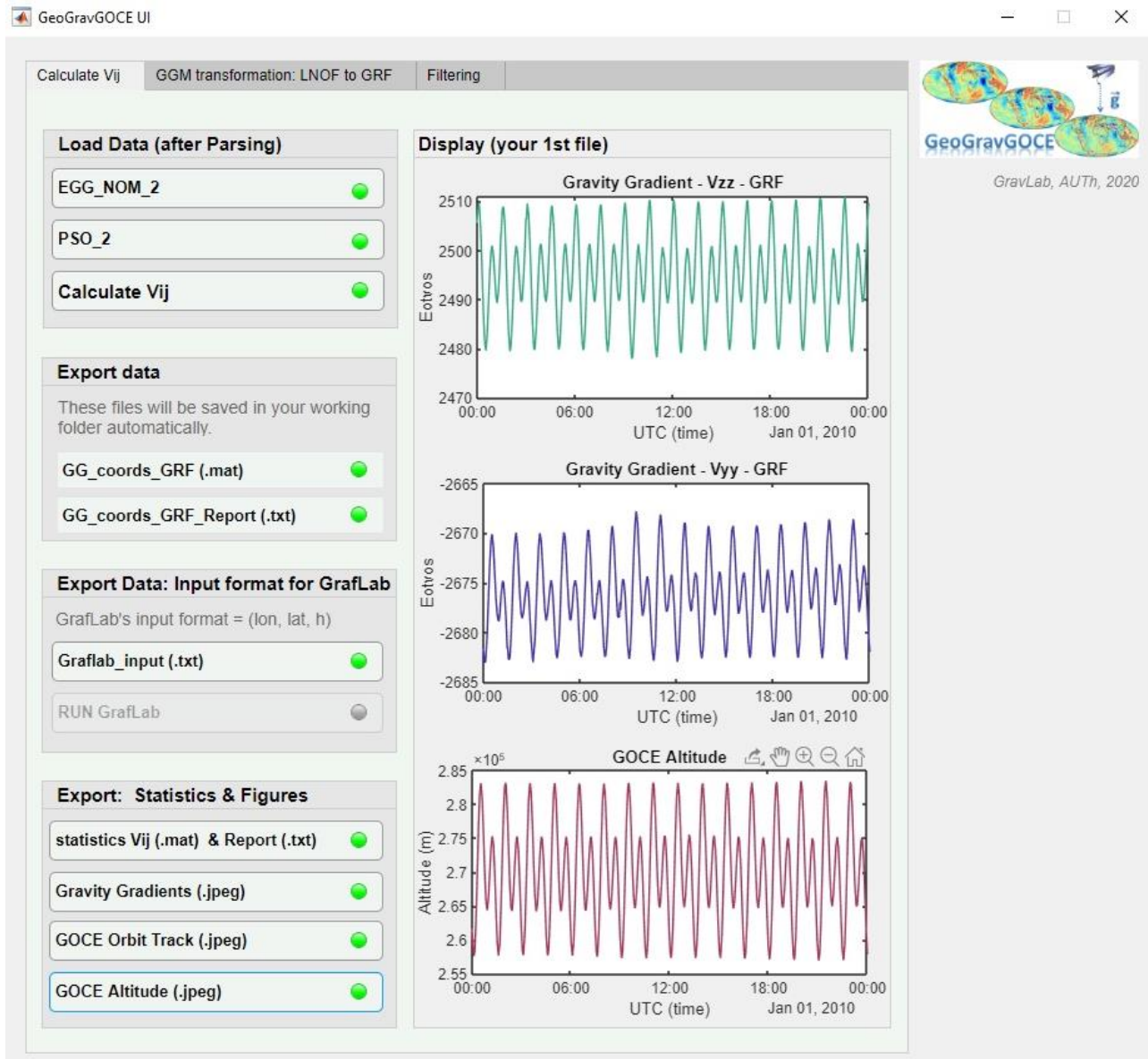

Figure 28: GUI's first tab

The user takes as output of the GUI a *.mat file and the corresponding report automatically, with all needed information, as shown in Figure 29.

```
  1
  2  GeoGravGOCE, GravLab, AUTh, 2020
  3
  4
  5  After "Calculation Vij button" You take as a return two files:
  6  [1]=GG_Coords_GRF.mat, cell=(18x1)
  7  [2]=GG_Coords_GRF_Report.mat
  8
  9  The format of the output "GG_Coords_GRF.mat":
 10  cells:
 11  GG_Coords_GRF{1} = longtitude (degrees) (GRS80)
 12  GG_Coords_GRF{2} = latitude (degrees) (GRS80)
 13  GG_Coords_GRF{3} = h (meter)(GOCE altitude)
 14  GG_Coords_GRF{4} = Vxx (Eotvos)[condition: length(NOM)=length(PSO)]
 15  GG_Coords_GRF{5} = Vyy (Eotvos)  -//-
 16  GG_Coords_GRF{6} = Vzz (Eotvos)  -//-
 17  GG_Coords_GRF{7} = Vxy (Eotvos)  -//-
 18  GG_Coords_GRF{8} = Vxz (Eotvos)  -//-
 19  GG_Coords_GRF{9} = Vzy (Eotvos)  -//-
 20  GG_Coords_GRF{10} = percentage (%) of lost data NOM, to correspond length(NOM)= length(PSO)
 21  GG_Coords_GRF{11} = UTC time (NOM data)
 22  GG_Coords_GRF{12} = The name of the current NOM day/file you process
 23  GG_Coords_GRF{13} = q1, quaternion GRF [condition: length(NOM)=length(PSO)]
 24  GG_Coords_GRF{14} = q2, quaternion GRF  -//-
 25  GG_Coords_GRF{15} = q3, quaternion GRF   -//-
 26  GG_Coords_GRF{16} = q4, quaternion GRF    -//-
 27  GG_Coords_GRF{17} = GPS time from EGG_NOM_2 data
 28  GG_Coords_GRF{18} = GPS time from PSO_2 data
 29  each of the 18 cells above contains N interiors cells, N= number of files you processed in the GUI
 30
```

Figure 29: The Report of the first tab's output

The second tab of GUI concerns the transformation of the geopotential model from LNOF to GRF. The user needs to import the gravity gradients in LNOF that are the output of Graflab (Bucha and Janák 2013) for the day/s he/she wants to transform as well as the SST_PSO_2 (.qat) file/s of the same day/s containing the quaternions needed for transformation from EFRF to IRF. By pressing the Transform LNOF to GRF button, the transformation from LNOF to GRF begins. When the process is over in the Display bar, the V_{zz} gradient of the first file in all four reference systems (LNOF, EFRF, IRF and GRF) will appear, while in the working folder of the user a .mat file containing the values of the six gradients in the systems will be saved automatically along with an associated report text file. In case the user chooses to, the statistics and the figures of the gravity gradients in GRF can be saved with the respected buttons. Figure 30 presents the Transformation tab in the Graphical User Interface.

Figure 30: GUI's second tab

1.9   Concluding remarks

All GeoGravGOCE needed DLs have been prepared until now and the work on the DLs foreseen for the near future is in good shape. Of importance is that the GOCE SGG data pre-processing has been standardized, the GRF-LNOF and reverse LNOF-GRF transformation have been implemented, the evaluation of the GGMs is underway and the reference to be used herein has been selected, various filtering methods have been tested and assessed in both the un-reduced and reduced observations, and finally a coherent GUI platform has been developed including all developed sub-routines for the data pre- and post-processing.

References

Bucha, Blažej and Juraj Janák. 2013. "A MATLAB-Based Graphical User Interface Program for Computing Functionals of the Geopotential up to Ultra-High Degrees and Orders." *Computers and Geosciences*.

Daubechies, Ingrid. 1992. *Ten Lectures on Wavelets*.

ESA. 2014. *GOCE High Level Processing Facility GOCE Level 2 Product Data Handbook*.

Grebenitcharsky, Rossen and Philip Moore. 2014. "Application of Wavelets for Along-Track Multi-Resolution Analysis of GOCE SGG Data." in *International Association of Geodesy Symposia*.

Grout, Ion. 2008. *Digital Systems Design with FPGAs and CPLDs*.

Jarecki, Focke, Karen Insa Wolf, Heiner Denker, and Jürgen Müller. 2006. "Quality Assessment of GOCE Gradients." *Observation of the Earth System from Space* (November):271–85.

Krasbutter, Ina, Jan Martin Brockmann, Boris Kargoll, and Wolf-Dieter Schuh. 2014. "Adjustment of Digital Filters for Decorrelation of GOCE SGG Data." 109–14.

Mallat, Stephane G. 1989. "A Theory for Multiresolution Signal Decomposition: The Wavelet Representation." *IEEE Transactions on Pattern Analysis and Machine Intelligence*.

Wan, Xiao Yun, Jin Hai Yu, and Yan Yan Zeng. 2012. "Frequency Analysis and Filtering Processing of Gravity Gradients Data from GOCE." *Acta Geophysica Sinica* 55(9):2909–16.